ISSN 1392-1207. MECHANIKA. Vol. 32, No. 5, 2026: 359–368

Elastoplastic Torsion of a Surface-Hardened Functionally Graded Square Bar with Spatially Varying Mechanical Properties

Javlonbek E. TURDIBEKOV, Rustam A. ABIROV, Farkhadjan F. ADILOV

Institute of Mechanics and Seismic Stability of Structures named after M.T. Urazbaev, Uzbekistan Academy of Sciences, Tashkent, Uzbekistan, E-mails: javlonbekturdibekov9@gmail.com, rustam.abirov@gmail.com, mahzun86@gmail.com

https://doi.org/10.5755/j02.mech.45547

1. Introduction

Torsion of prismatic bars is a classical problem in solid mechanics. Elastic solutions commonly use Saint-Venant's semi-inverse method with either a warping function or Prandtl's stress function. Elastoplastic torsion is more complex because the stress and strain distributions depend on cross-sectional geometry, constitutive behavior, and loading history.

Elastoplastic torsion of homogeneous bars under combined loading has been studied in [1, 2], while integral formulations for homogeneous cylindrical specimens under complex loading are presented in [3]. Boundary integral approaches determine unknown stresses and displacements from boundary quantities. Finite difference formulations resolve the entire cross-section, facilitating analysis of the evolving stress-strain state.

While the Finite Element Method (FEM) is dominant in standard structural software, it faces significant meshing challenges when handling severe continuous material gradients. Thus, a customized Finite Difference Method (FDM) utilizing control volumes is much more suitable for capturing smooth property variations directly inside the differential operator without step-like approximations.

Numerical analyses of dispersion-strengthened materials were reported [4], while the combined influence of cross-sectional topology and axial–torsional loading sequence on elastoplastic stress redistribution and effective torsional stiffness was investigated in [5].

In many engineering applications, however, structural materials cannot be regarded as either homogeneous or isotropic. Surface treatment processes such as carburizing produce gradual variations in the mechanical properties through the thickness of the material. At the same time, increasingly stringent engineering requirements have stimulated the development and application of functionally graded materials (FGMs), whose continuously varying composition enables the mechanical response to be tailored to specific service conditions.

The use of functionally graded materials in engineering structures requires a thorough understanding of their mechanical behavior under different loading conditions. Owing to their hierarchical architecture and multifunctional properties, FGMs provide new opportunities for material design and advanced manufacturing aimed at meeting modern technological requirements [6]. In addition, fracture processes in FGMs have attracted considerable attention because spatial variations in material properties significantly influence the stress intensity factors and may substantially improve fracture resistance [7].

Previous studies have examined the distribution of shear stresses in functionally graded bars subjected to pure torsion for cross-sections of various geometries and thicknesses [8]. A new boundary integral formulation for the elastoplastic torsion of functionally graded bars with arbitrary cross-sections was proposed in Ref. [9], where the effective properties of a two-phase functionally graded material were evaluated using a homogenization scheme.

Wave propagation in functionally graded materials has also attracted considerable interest. It has been shown that the amplitude characteristics of elastic waves can be effectively controlled by varying the thickness of the graded layer [10]. Furthermore, FGMs may be modeled as heterogeneous composites formed by combining two constituent materials with continuously varying composition. Longitudinal wave propagation in rods with axial material gradation has been investigated [11].

The material considered in the present study possesses a hardened outer layer capable of sustaining high surface loads, whereas the core remains relatively ductile. Such a configuration cannot be adequately represented using constant values of the shear modulus and yield stress throughout the cross-section. Therefore, the shear modulus, yield stress, and strain-hardening parameter are assumed to be coordinate-dependent material functions.

A distinctive feature of the proposed model is that plastic yielding does not necessarily initiate at the locations where the shear stresses attain their maximum values. Instead, the onset of plastic deformation is governed by the interaction between the local stress field and the spatial variation of the material properties. The primary objective of this study is to quantify the influence of different combinations of graded material properties on the evolution of plastic zones in a surface-hardened square bar subjected to Saint-Venant torsion, with particular emphasis on the effects of spatially varying yield stress and the thickness of the initially hardened surface layer.

2. Problem Formulation and Methodology

Consider a prismatic bar with a square cross-section (Fig. 1) occupying the domain

$$\Omega = \left\{ (x, y) : -a \le x \le a, -a \le y \le a \right\}. \tag{1}$$

The bar is subjected to Saint-Venant torsion about the longitudinal z-axis. A dimensionless twist parameter is introduced as

$$\beta = \frac{\alpha \cdot a}{\varepsilon_{y,c}}, \tag{2}$$

where α denotes the twist per unit length and $\varepsilon_{0,C}$ is the reference yield strain of the core material.

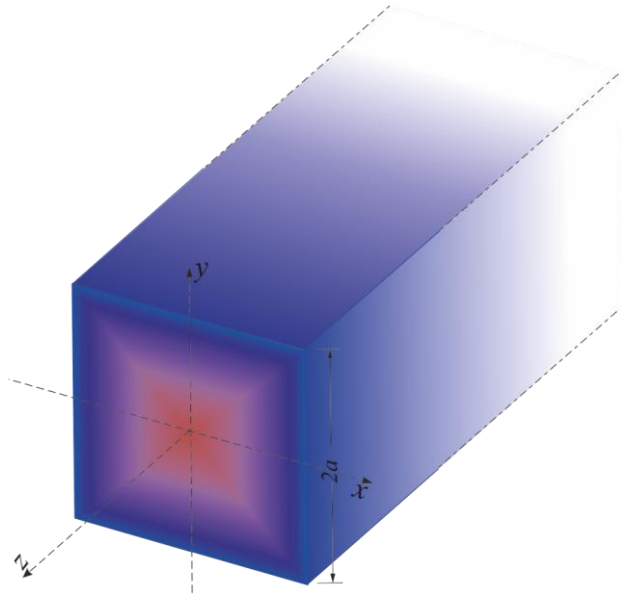

Fig. 1 Surface-hardened functionally graded square bar with a ductile core subjected to elastoplastic torsion

To describe the spatial variation of the material properties, the distance from an arbitrary point within the cross-section to the external boundary is defined as

To preserve the pristine geometry of the square hardened layer and maintain contours strictly parallel to the outer boundary, the distance function $d(x, y)$ is formulated as:

$$d(x,y) = a - max\left(|x|,|y|\right). \tag{3}$$

According to Eq. (3), $d = 0$ at the outer boundary of the square and $d = a$ at the center of the cross-section. This definition is preferred over the conventional radial distance because it preserves the geometry of the hardened layer by maintaining contours parallel to the square boundary, thereby providing a physically consistent representation of surface hardening under torsion.

To ensure a smooth thermodynamic and mechanical transition without introducing artificial interface jump conditions, the following original auxiliary transition function H(d) is adopted as:

$$H(d) = \frac{1}{2}\left[1 - th\left(\frac{d - t_s}{\delta_s}\right)\right]. \tag{4}$$

At $d < t_s$, the argument of the hyperbolic tangent is negative and $H \to 1$, corresponding to the hardened surface layer. Conversely, at $d > t_s$, $H \to 0$, representing the core material. At $d = t_s$, the transition function satisfies $H = 0.5$. Here, t_s denotes the nominal depth of the hardened layer, while δ_s controls the smoothness of the material transition. The continuous representation adopted in Eq. (4) eliminates discontinuities in the material properties and avoids the need for additional interface jump conditions at the initial stage of the numerical formulation.

The evaluation of the equivalent plastic strain is performed using the incremental theory of plasticity, adapted for spatially varying parameters in the following form:

$$\varepsilon_{et}^{p} = \frac{\varepsilon_{et}(x,y) - \dfrac{\sigma_y(x,y)}{G(x,y)}}{1 + \dfrac{2}{3}(1+\nu)\dfrac{m(x,y)}{1-m(x,y)}}, \tag{5}$$

where ν is Poisson's ratio, σ_y is the yield stress, $m = H / G$ is the hardening parameter, and H denotes the plastic hardening modulus.

Eq. (5) plays a fundamental role in the proposed formulation. Since both the shear modulus G and the yield stress σ_y vary spatially, the onset and evolution of plastic deformation become coordinate dependent throughout the cross-section. The denominator of Eq. (5) contains the strain-hardening parameter. Consequently, an increase in m_h leads to a reduction in the accumulated plastic strain.

The spatially varying mechanical properties are expressed through the transition function $H(d)$ as

$$G(x,y) = G_c\left[1 + (R_G - 1)H(d)\right], \tag{6}$$

$$\sigma_y(x,y) = \sigma_{y,c}\left[1 + (R_y - 1)H(d)\right], \tag{7}$$

$$m_h(x,y) = m_c + (m_s - m_c)H(d). \tag{8}$$

Here, $R_G = G_s / G_c$ and $R_y = \sigma_{y,s} / \sigma_{y,c}$; the subscripts s and c denote the surface layer and the core, respectively.

Eqs. (6)-(8) ensure that the material properties continuously approach the core values as $H \to 0$ and the surface values as $H \to 1$. The homogeneous material is recovered as the limiting case

$$R_G = 1, \quad R_y = 1, \quad m_s = m_c. \tag{9}$$

The reference material parameters adopted throughout this study are:

$$\frac{t_s}{a} = 0.20, \quad \frac{\delta_s}{a} = 0.035, \quad R_y = 1.60,$$
$$R_G = 1.15, \quad m_c = 0.05, \quad m_s = 0.10. \tag{10}$$

The value $R_y = 1.6$ indicates that the yield stress of the hardened surface layer exceeds that of the core by 60%. Likewise, $R_G = 1.15$ implies that the shear modulus at the outer surface is 15% greater than that of the core. Such a combination is mechanically realistic for surface-hardened metallic components, in which the yield strength may increase substantially, whereas the elastic modulus generally exhibits only moderate variations (Fig. 2).

Fig. 2 illustrates the distribution of the transition function $H(d)$ together with the corresponding variations of

the mechanical properties across the cross-section for the reference transition parameter $\delta_s / a = 0.035$.

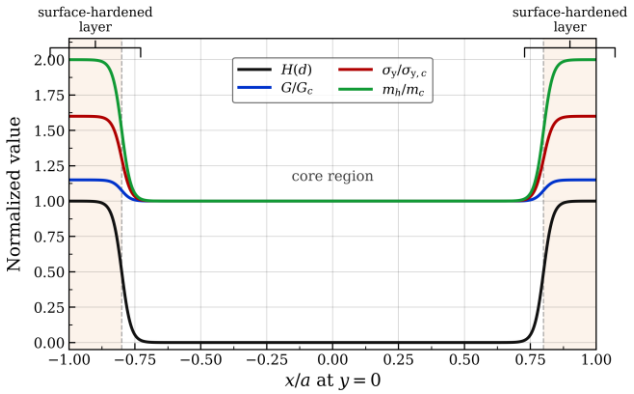

Fig. 2 Spatial variation of the transition function and the corresponding material properties across the cross-section

3. Governing Equation for Torsion with Spatially Varying Material Properties

Let $\omega(x, y)$ denote the warping function. According to the classical Saint-Venant torsion framework, assuming small deformations, the kinematic relations are

$$\varepsilon_{xz} = \frac{1}{2}\left(-\alpha y + \frac{\partial \omega}{\partial x}\right), \qquad \varepsilon_{yz} = \frac{1}{2}\left(\alpha x + \frac{\partial \omega}{\partial y}\right). \tag{11}$$

The relations in Eq. (11) are purely kinematic and therefore remain valid for both homogeneous and spatially heterogeneous materials.

The equivalent shear strain is defined as

$$\varepsilon_{et} = \frac{2}{\sqrt{3}}\sqrt{\varepsilon_{xz}^2 + \varepsilon_{yz}^2}. \tag{12}$$

Within the elastic regime, the constitutive equations are:

$$\tau_{xz} = 2G\varepsilon_{xz}, \qquad \tau_{yz} = 2G\varepsilon_{yz}. \tag{13}$$

Substituting Eq. (13) into the von Mises equivalent stress expression yields:

$$\sigma_e = \sqrt{3}\sqrt{\tau_{xz}^2 + \tau_{yz}^2} = 3G\varepsilon_{et}. \tag{14}$$

According to the von Mises yield criterion expressed in terms of strains, the local equivalent yield strain is given by:

$$\varepsilon_{et}^0(x,y) = \frac{\sigma_y(x,y)}{3G(x,y)}. \tag{15}$$

The plastic strain components are assumed to be proportional to the total strain components,

$$\varepsilon_{xz}^p = \frac{\varepsilon_p}{\varepsilon_{et}}\varepsilon_{xz}, \qquad \varepsilon_{yz}^p = \frac{\varepsilon_p}{\varepsilon_{et}}\varepsilon_{yz}, \tag{16}$$

where these expressions are applicable only for $\varepsilon_{et} > 0$.

The stress components in the elastoplastic regime are therefore written as

$$\begin{aligned} \tau_{xz} &= 2G(x,y)\left(\varepsilon_{xz} - \varepsilon_{xz}^p\right), \\ \tau_{yz} &= 2G(x,y)\left(\varepsilon_{yz} - \varepsilon_{xz}^p\right). \end{aligned} \tag{17}$$

To characterize the local state of plastic loading, the loading coefficient (yield index) is introduced as

$$\eta(x,y) = \frac{\sigma_e(x,y)}{\sigma_y(x,y)}, \text{ here } \sigma_e = \sqrt{3}\sqrt{\tau_{xz}^2 + \tau_{xz}^2}. \tag{18}$$

According to Eq. (18), the condition $\eta(x, y) = 1$ corresponds to the onset of yielding. For a homogeneous material, where the yield stress $\sigma_y(x, y)$ is constant throughout the cross-section, the maximum value of $\eta(x, y)$ coincides with the maximum equivalent stress $\sigma_e(x, y)$. This statement no longer holds for functionally graded materials. A point located near the surface may experience relatively high shear stresses while remaining entirely within the elastic regime because of its elevated local yield strength. Consequently, the loading coefficient (yield index) η provides a more informative measure of the degree of plastic development than the stress field alone.

The equilibrium equation for Saint-Venant torsion is:

$$\frac{\partial \tau_{xz}}{\partial x} + \frac{\partial \tau_{yz}}{\partial y} = 0. \tag{19}$$

Substituting Eqs. (11) and (17) into Eq. (19) yields:

$$\frac{\partial}{\partial x}\left[G(x,y)\left(\frac{\partial \omega}{\partial x} - \alpha y - 2\varepsilon_{xz}^p\right)\right] + \frac{\partial}{\partial y}\left[G(x,y)\left(\frac{\partial \omega}{\partial y} + \alpha x - 2\varepsilon_{yz}^p\right)\right] = 0. \tag{20}$$

Eq. (20) constitutes the governing equation of the present study. Unlike the classical Poisson equation, its coefficients are spatially variable because both the shear modulus $G = G(x, y)$ and the plastic strain field depend on position within the cross-section.

For compact notation, introduce the vector:

$$\boldsymbol{b} = \begin{pmatrix} \alpha y + 2\varepsilon_{xz}^p \\ -\alpha x + 2\varepsilon_{yz}^p \end{pmatrix}. \tag{21}$$

Eq. (20) can then be rewritten in divergence form as:

$$\nabla \cdot \left\{G(x,y)\left[\nabla \omega - \boldsymbol{b}\right]\right\} = 0. \tag{22}$$

The lateral surface of the bar is assumed to be traction-free,

$$\tau_{xz} n_x + \tau_{yz} n_y = 0, \tag{23}$$

which, upon substitution of Eqs. (11) and (17), leads to the Neumann boundary condition:

$$\frac{\partial \omega}{\partial n} = \boldsymbol{b} \cdot \boldsymbol{n} = \alpha\left(n_x y - n_y x\right) + 2\left(n_x \varepsilon_{xz}^p + n_y \varepsilon_{yz}^p\right). \quad (24)$$

Although the shear modulus G does not appear explicitly in the boundary condition, it continues to govern the solution through the differential operator in Eq. (22). Finally, to ensure the uniqueness of the Neumann problem, the following normalization condition is imposed:

$$\int_{\boldsymbol{R}} \omega \cdot dA = 0. \quad (25)$$

4. Finite Difference Formulation

In this study, a Finite Difference Method (FDM) layout based on a structured uniform grid and node-centered control volumes is deployed, rather than traditional Finite Element Analysis (FEA).

The square computational domain is discretized into an N×N array of control volumes with a uniform grid spacing:

$$h = \frac{2a}{N},\ x_i = -a + \left(i + \frac{1}{2}\right)h,\ y_j = -a + \left(j + \frac{1}{2}\right)h. \quad (26)$$

To determine the unknown warping function ω, Eq. (22) is integrated over each control volume. Applying the integral form of the equilibrium equation yields the flux balance

$$\Phi_E - \Phi_W + \Phi_N - \Phi_S = 0, \quad (27)$$

where the fluxes through the eastern, western, northern, and southern faces of the control volume are approximated by finite differences as:

$$\Phi_E = G_E\left(\frac{\omega_{i+1,j} - \omega_{ij}}{h} - b_{x,E}\right)h, \qquad \Phi_N = G_N\left(\frac{\omega_{i,j+1} - \omega_{ij}}{h} - b_{y,N}\right)h,$$
$$\Phi_W = G_W\left(\frac{\omega_{i+1,j} - \omega_{ij}}{h} - b_{x,W}\right)h, \qquad \Phi_S = G_S\left(\frac{\omega_{i,j+1} - \omega_{ij}}{h} - b_{y,S}\right)h. \quad (28)$$

Because the shear modulus varies throughout the cross-section, its value at the cell faces is evaluated using the harmonic average:

$$G_{i+1/2,j} = \frac{2G_{ij}G_{i+1,j}}{G_{ij} + G_{i+1,j}}. \quad (29)$$

The harmonic interpolation preserves the continuity of the shear modulus across adjacent control volumes and provides an accurate approximation of the variable-coefficient operator.

The discretization represented by Eqs. (27)-(28) produces, at each plastic iteration, the linear algebraic system

$$A\omega = r. \quad (30)$$

Since all boundary conditions are of Neumann type, the resulting system is singular up to an arbitrary additive constant. Rather than fixing the value of the warping function at an arbitrary node, the normalization condition in Eq. (25) is imposed through the augmented system. To enforce the uniqueness of the Neumann boundary problem and eliminate the singular null-space of the system matrix without placing an artificial rigid constraint on a single node, the integral condition Eq. (25) is directly embedded into the global system matrix via an augmented bordered matrix formulation

$$\begin{bmatrix} A & c \\ c^T & 0 \end{bmatrix}\begin{bmatrix} \omega \\ \lambda \end{bmatrix} = \begin{bmatrix} r \\ 0 \end{bmatrix}, \quad (31)$$

where $c = \left(h^2, h^2, ..., h^2\right)^T$.

This approach eliminates the null space without introducing an artificial constraint and is therefore more appropriate for the numerical solution of the warping function.

The nonlinear problem is solved by an iterative procedure. At the k-th iteration, the vector $\boldsymbol{b}^k$ is evaluated using the current plastic strain field. Eq. (22) is then solved for the updated warping function ω^{k+1}, after which the strain components given by Eqs. (11) are recalculated. Finally, the plastic strains are updated according to Eqs. (5) and (16).

To improve the numerical stability of the nonlinear iterations, an under-relaxation scheme is employed:

$$\left(\varepsilon_{xz}^p\right)^{k+1} = (1-\lambda)\left(\varepsilon_{xz}^p\right)^k + \lambda\left(\hat{\varepsilon}_{xz}^p\right)^{k+1},$$
$$\left(\varepsilon_{yz}^p\right)^{k+1} = (1-\lambda)\left(\varepsilon_{yz}^p\right)^k + \lambda\left(\hat{\varepsilon}_{yz}^p\right)^{k+1}, \quad (32)$$

where λ is the relaxation parameter.

The iterative process is considered converged when:

$$E_p^{(k)} < 10^{-4}, \qquad E_M^{(k)} < 10^{-4}, \quad (33)$$

where $E_p^{(k)}$ denotes the average change in the plastic strain vector over all computational cells, and $E_M^{(k)}$ represents the relative change in the dimensionless torque.

The following dimensionless quantities are used throughout the paper:

$$M^* = \frac{|M|}{2G_c\varepsilon_{0,c}a^3},\ M = \int_\Omega \left(x\tau_{yz} - y\tau_{xz}\right)dA, \quad (34)$$

$$\tau_{max}^* = \frac{\max_\Omega \sqrt{\tau_{xz}^2 + \tau_{yz}^2}}{2G_c\varepsilon_{0,c}}, \quad (35)$$

$$\frac{A_p}{A} = \frac{cells\ area\ with\ \ \varepsilon_p > 0}{total\ area\ of\ cross-section}. \quad (36)$$

These dimensionless parameters are used throughout the following sections to evaluate the torsional response, the evolution of the plastic zone, and the influence of spatially varying material properties.

The proposed finite difference formulation is particularly suitable for problems involving spatially varying material properties because variable coefficients are incorporated directly into the governing equation without requiring additional interface conditions. Furthermore, the use of harmonic averaging ensures a stable and accurate representation of material gradients across adjacent control volumes.

5. Calculation Scheme

To ground the numerical model in engineering reality, the core material functions are calibrated based on a low-carbon alloy steel subjected to surface carburization. For core $G_c = 80$ GPa, $\sigma_{y,c} = 400$ MPa. For surface layer $R_y = 1.6$, $\sigma_{y,s} = 640$ MPa.

The baseline configuration represents a high-strength low-carbon alloy steel subjected to surface carburization and subsequent heat treatment. The nominal core parameters are shear modulus $G_c = 80$ GPa and initial yield stress $\sigma_{y,c} = 400$ MPa. For the reference ratios in Eq. (10) $R_y = 1.6$, $R_G = 1.15$, the physical properties at the absolute outer surface are scaled to $G_c = 92$ GPa and $\sigma_{y,s} = 640$ MPa, representing increased yield strength with a moderate change in elastic stiffness.

The numerical simulations were carried out by varying the material parameters listed in Table 1. The homogeneous material defined by Eq. (9) was retained as the reference case. The baseline functionally graded material corresponds to the parameter set given by Eq. (10). In all subsequent numerical experiments, only a single material parameter was varied while the remaining parameters were kept unchanged. Specifically, the influence of the hardened layer thickness, the yield stress ratio, and the strain-hardening parameter was investigated independently. Such a one-factor-at-a-time strategy eliminates ambiguity in interpreting the numerical results and allows the contribution of each design parameter to be evaluated separately.

Table 1

Material parameters considered in the numerical study

Case	Purpose	t_s/a	δ_s/a	R_y	R_G	m_c	m_s
Homogeneous	control	0.2	0.035	1	1	0.05	0.05
Baseline	reference FGM	0.2	0.035	1.6	1.15	0.05	0.1
$t_s = 0.10$	hardened-layer thickness	0.1	0.035	1.6	1.15	0.05	0.1
t_s=0.30	hardened-layer thickness	0.3	0.035	1.6	1.15	0.05	0.1
R_y=1.20	yield-stress contrast	0.2	0.035	1.2	1.15	0.05	0.1
R_y =2.00	yield-stress contrast	0.2	0.035	2	1.15	0.05	0.1
R_G=1.00	elastic-stiffness contrast	0.2	0.035	1.6	1	0.05	0.1
R_G=1.30	elastic-stiffness contrast	0.2	0.035	1.6	1.3	0.05	0.1

Grid convergence was examined using computational meshes with $N = 41$, 81, 121, and 161. The numerical results presented below correspond to the finest mesh ($N = 161$), which was adopted as the reference solution. The numerical investigation addresses four principal engineering questions:

1. How does a functionally graded material differ from a homogeneous material under torsion?
2. What is the influence of the hardened layer thickness?
3. How does the spatial variation of yield stress affect the evolution of plasticity?
4. What is the influence of the spatial variation of the shear modulus?

6. Comparison Between Homogeneous and Functionally Graded Bars

Fig. 3 compares the response of the homogeneous material defined by Eq. (9) with that of the reference functionally graded material described by Eq. (10). Three quantities are considered: the dimensionless torque, the maximum yield index, and the relative area of the plastic zone.

At the twist level $\beta = 2$, the principal response parameters change as follows:

$$M^*:\ 1.8146 \to 2.3039,\quad +26.97\%,$$
$$\tau^*_{max}:\ 0.7973 \to 1.2576,\quad +57.74\%,$$
$$\eta_{max}:\ 1.0457 \to 1.0354,\quad -0.99\%,$$
$$\varepsilon^p_{max}:\ 0.8603 \to 0.4390,\quad -48.98\%,$$
$$A_p / A:\ 0.3384 \to 0.2255, -33.38\%.$$

The increase in the maximum shear stress is attributed to the stronger hardened surface layer, which carries a larger portion of the applied torque. Nevertheless, the maximum yield index remains almost unchanged (Fig. 3). This observation demonstrates that, for functionally graded materials, stress magnitudes alone are insufficient to characterize the mechanical response. The degree of plastic development must also be evaluated through the yield index.

At the higher twist level $\beta = 6$,
M^*: 2.2303 → 2.9626, +32.83%, while
ε^p_{max}: 4.5694 → 3.8825, −15.3%.

At this stage, the plastic-zone fractions become nearly identical because both materials have entered a fully developed plastic regime. Therefore, the beneficial effect of the graded surface layer is most pronounced during the initiation and early evolution of plastic deformation and gradually diminishes as plasticity spreads throughout the cross-section.

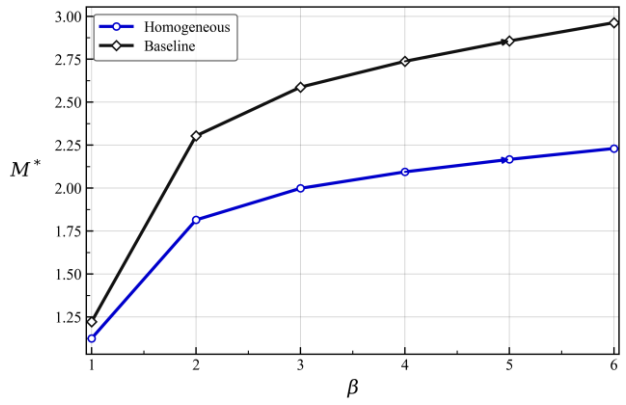

a

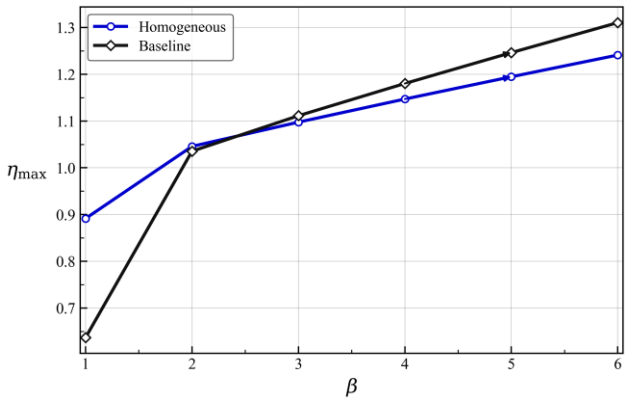

b

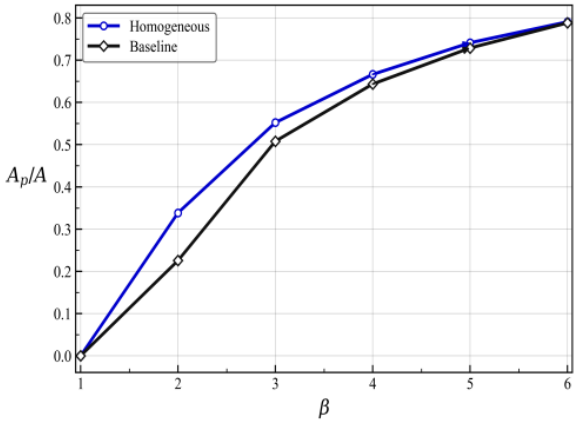

c

Fig. 3 Comparison between the homogeneous bar and the reference functionally graded bar: a – dimensionless torque; b – maximum yield index; c – relative plastic-zone area

The onset of yielding is determined from the condition $\eta_{max} = 1$.

Linear interpolation of the numerical curves yields: $\beta_y^{hom} = 1.704$, $\beta_y^{P0} = 1.911$.

Thus, the functionally graded material delays the initiation of yielding by approximately 12.2% relative to the homogeneous bar. This represents one of the principal findings of the present study.

Direct experimental validation of elastoplastic stress-strain tensors inside functionally graded square bars remains extremely difficult due to the inability of physical sensors to capture internal continuous deformation fields without destroying the specimen. Therefore, to evaluate the mathematical accuracy and numerical stability of the proposed finite difference code, a strict verification study was conducted via material property reduction. By setting $R_y = 1.0$, $R_G = 1.0$, and $m_c = m_s = 0.05$, the functionally graded model degenerates into a classical homogeneous elastoplastic bar. The numerical torque-twist curve $M^* - \beta$ generated by the refined 161 × 161 grid was directly compared against the well-established semi-analytical and numerical results provided by Tsiatas & Babouskos [9] and classical elastoplastic torsion benchmarks. The maximum relative discrepancy in torque values across the entire loading range ($\beta = 1$ to 6) did not exceed 0.42%, which rigorously confirms the mathematical validity of the developed algorithm, grid independence, and face flux balancing.

7. Stress and Plastic-Strain Distributions

Fig. 4 presents the distributions of the yield index and plastic strain over the cross-section for the reference functionally graded material at $\beta = 6$.

The yield index provides considerably more information than the shear-stress contours because it quantifies the proximity of the local stress state to yielding while accounting for spatial variations in the yield stress. Consequently, it serves as a direct indicator of the local degree of

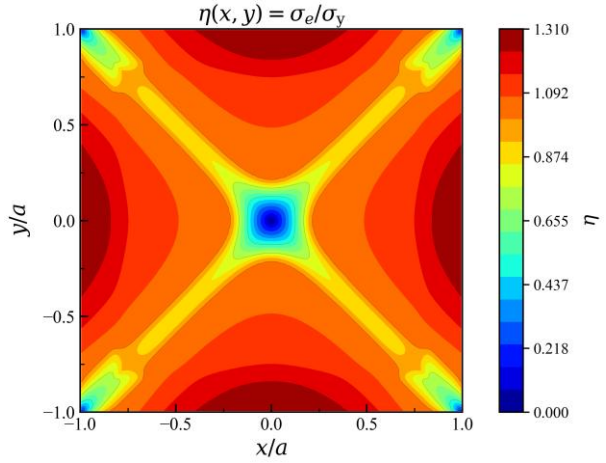

a

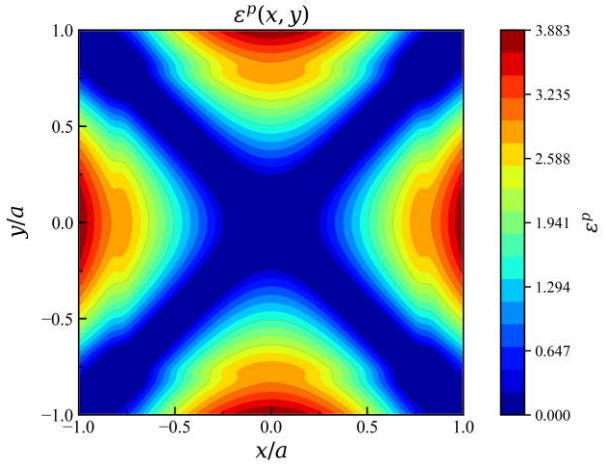

b

Fig. 4 Distribution over the cross-section: a – yield index; b – equivalent plastic strain

plastic development.

By contrast, the shear stress alone cannot distinguish between regions that have undergone substantial hardening and those that remain elastic. Therefore, for functionally graded materials, the most critical regions should be identified using the yield index rather than the shear stress alone.

The plastic-strain distribution further demonstrates that the hardened surface layer does more than merely increase torsional stiffness. It significantly modifies the geometry and evolution of the plastic zone. This influence is particularly pronounced during the initial stages of yielding. As plastic deformation progresses, the plastic region spreads over most of the cross-section, and the distinction between the hardened layer and the ductile core gradually diminishes.

8. Influence of the Hardened Layer Thickness

The influence of the hardened layer thickness on the development of plastic deformation was investigated by considering three values of the normalized layer thickness, $t_s / a = 0.1,\ 0.2,\ 0.3$ while keeping the remaining material parameters constant, $R_y = 1.60$, $R_G = 1.15$.

The maximum yield index, η_{max}, and the relative plastic-zone area, A_p / A, were selected as the principal response parameters because they provide a direct measure of the extent of plastic deformation and, consequently, of the effectiveness of the hardened surface layer. The corresponding results are shown in Fig. 5.

At the early stage of loading ($\beta = 2$), increasing the normalized hardened layer thickness from t_s / a=0.10 to 0.30 increases the dimensionless torque by 14.82%, reduces the maximum plastic strain by 27.04%, and decreases the relative plastic-zone area by 55.21%.

The reduction in the plastic zone may be quantified by $\dfrac{\left(A_p / A\right)_{t_s/a=0.10}}{\left(A_p / A\right)_{t_s/a=0.30}} \approx 2.23$.

Thus, at the onset of plastic deformation, increasing the hardened layer thickness reduces the plastically deformed area by approximately 2.2 times.

This result demonstrates that the hardened layer acts as an effective barrier against the inward propagation of plastic deformation. A thicker surface layer redistributes the applied torque more efficiently, delaying yielding within the ductile core.

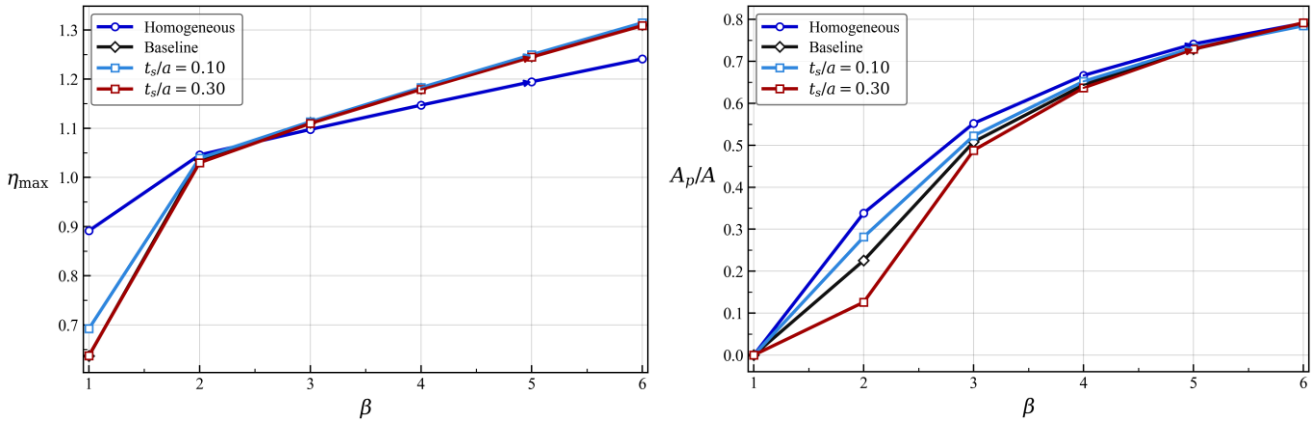

Fig. 5 Influence of the hardened layer thickness on the evolution of plasticity: a – maximum yield index; b – relative plastic-zone area

As the applied twist increases ($\beta = 6$), the influence of the hardened layer thickness becomes considerably less pronounced. For the same increase in ts/a, the dimensionless torque rises by 21.16%, whereas the maximum plastic strain decreases by only 1.98%, and the plastic-zone area changes by less than 1%.

This behavior indicates that, once extensive plastic deformation has developed throughout the cross-section, the beneficial effect of increasing the hardened layer thickness gradually diminishes. At this stage, the mechanical response is governed primarily by the plastic behavior of the entire cross-section rather than by the properties of the surface layer.

From an engineering standpoint, these results suggest that increasing the thickness of the hardened layer is an effective strategy for delaying the initiation and early propagation of plastic deformation. However, when structural components are expected to operate under severe plastic loading, increasing the hardened layer thickness alone cannot ensure a substantial improvement in structural safety.

9. Influence of the Yield Stress Gradient

The second series of numerical simulations examines the influence of the yield stress ratio between the hardened surface layer and the core. Three values were considered, $R_y = 1.2,\ 1.6,\ 2.0$ while maintaining $t_s / a = 0.20$, $R_G = 1.15$.

Among all material parameters, the yield stress ratio is expected to have the greatest influence on plastic deformation because the onset of yielding is governed directly by the ratio between the equivalent stress and the local yield stress. The corresponding results are shown in Fig. 6.

The numerical results demonstrate a consistent and physically meaningful trend. As the yield stress contrast increases, the plastic zone develops more slowly, whereas the torque-carrying capacity increases.

For the strongest material gradient ($R_y = 2$), compared with the reference case ($R_y = 1.6$) at $\beta = 2$, the dimensionless torque increases by 5.28%, whereas the maximum yield index decreases by 2.70%, the maximum plastic strain

decreases by 68.68%, and the plastic-zone area decreases by 59.07%.

A direct comparison between the weakest and strongest gradients gives

$$\frac{\left(\varepsilon^p_{max}\right)_{R_y=1.20}}{\left(\varepsilon^p_{max}\right)_{R_y=2.00}} \approx 5.52 \text{ and } \frac{\left(A_p / A\right)_{R_y=1.20}}{\left(A_p / A\right)_{R_y=2.00}} \approx 3.57 .$$

Therefore, increasing the yield stress ratio from 1.20 to 2.00 reduces the maximum plastic strain by more than a factor of five and decreases the plastically deformed area by approximately 3.6 times during the initial stage of plastic deformation.

The onset of yielding exhibits the same tendency. Linear interpolation of the numerical results gives $\beta_y\,(R_y = 1.20) = 1.65$, $\beta_y\,(R_y = 2.00) = 1.983$.

Compared with the homogeneous material, the largest yield stress gradient delays the initiation of yielding by approximately 16.4%, whereas the improvement relative to the reference configuration amounts to 3.75%.

These results clearly indicate that the spatial variation of the yield stress is the dominant material parameter governing the initiation and early evolution of plastic deformation. Among all parameters considered in the present study, the yield stress gradient has the strongest influence on the size and location of the plastic zone.

10. Influence of the Shear Modulus Gradient

The final series of simulations investigates the influence of the shear modulus ratio, $R_G = 1.00,\ 1.15,\ 1.30$, while keeping $t_s / a = 0.20$, $R_y = 1.60$.

The parameter R_G characterizes the relative stiffness of the hardened surface layer with respect to the ductile core. The corresponding results are shown in Fig. 7.

At $\beta = 2$, increasing the shear modulus ratio from $R_G = 1$ to $R_G = 1.3$ increases the dimensionless torque by 6.68%. However, the same increase also produces a 3.97% increase in the maximum yield index, a 213.8% increase in the maximum plastic strain, and an 87.79% increase in the plastic-zone area.

These changes may be expressed as

$$\frac{\left(\varepsilon^p_{max}\right)_{R_G=1.30}}{\left(\varepsilon^p_{max}\right)_{R_G=1.00}} \approx 3.14 \text{ and } \frac{\left(A_p / A\right)_{R_G=1.30}}{\left(A_p / A\right)_{R_G=1.00}} \approx 1.88 .$$

At higher loading levels ($\beta = 6$), the differences become less pronounced. The case $R_G = 1.3$ produces a dimensionless torque approximately 4% greater than that obtained for $R_G = 1$, while the maximum yield index remains approximately 8% higher.

Unlike the yield stress ratio, increasing the shear modulus does not suppress plastic deformation. Instead, the increased stiffness transfers a larger portion of the applied torque to the hardened surface layer, thereby increasing the local stress concentration. Consequently, although the torsional stiffness increases, the plastic deformation may also intensify.

These observations indicate that the shear modulus ratio should not be optimized independently. Instead,

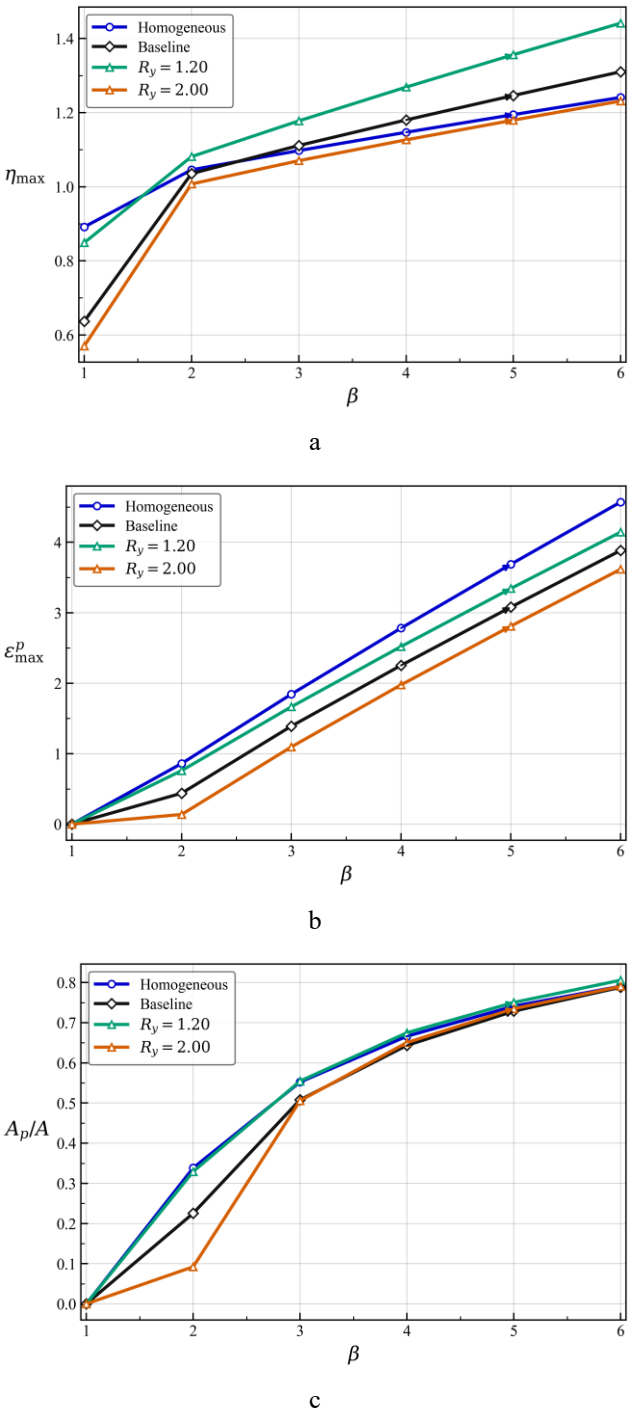

Fig. 6 Influence of the yield stress ratio on the development of plasticity: a – maximum yield index, b – maximum equivalent plastic strain, c – relative plastic-zone area

it must be considered together with the spatial distribution of the yield stress. A combination of a high yield stress and a moderately increased shear modulus provides the most favorable balance between torsional stiffness and resistance to plastic deformation.

11. Discussion

Previous studies report agreement between numerical predictions and experiments for elastoplastic torsion of homogeneous materials [12]. Torsion also produces a complex multiaxial stress state under nominally simple

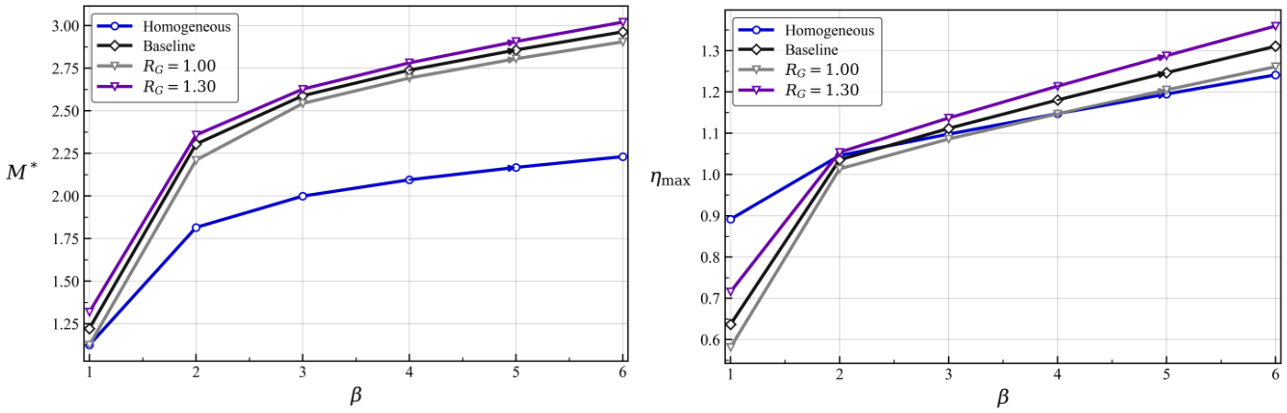

Fig. 7 Influence of the shear modulus ratio: a – dimensionless torque; b – maximum yield index

loading [13], leaving the applicability of constitutive models in the plastic regime open to investigation. Here, incremental deformation theory provides a computationally efficient description of functionally graded materials with spatially varying mechanical properties.

The graded layer most strongly reduces maximum plastic strain and plastic-zone extent during yielding initiation and early plastic loading. Its influence diminishes as plasticity spreads across the section, and the response approaches that of a fully plastic homogeneous material.

Greater layer thickness delays penetration toward the core and reduces plastic-zone area under moderate loading. Additional thickness gives only marginal benefit near the fully plastic state and cannot alone improve capacity under severe plastic deformation.

The yield stress ratio has the strongest influence of the parameters investigated. Increasing Ry delays yielding and reduces maximum plastic strain and plastic-zone size. Local yield strength, rather than the hardened layer alone, governs surface-hardening effectiveness.

A higher shear modulus ratio increases stiffness, transmitted torque, and local stress in the hardened region. Higher stiffness need not reduce plastic deformation; shear modulus and yield stress distributions should be optimized together to balance stiffness and resistance to plastic flow.

Yielding in graded materials need not begin at maximum shear stress. Spatially varying yield strength makes the local equivalent-stress-to-yield-strength ratio decisive. The yield index describes the local state more effectively than shear stress and distinguishes graded behavior from homogeneous behavior.

12. Conclusions

A numerical model has been developed for elastoplastic torsion of a surface-hardened functionally graded square bar. Spatially varying shear modulus, yield stress, and strain-hardening parameter represent the graded response more realistically than a homogeneous model.

The principal conclusions are as follows:

1. The graded layer changes torsional stiffness and plastic-zone evolution. Interaction between local stresses and spatially varying material properties redistributes plastic deformation across the section.

2. Yielding need not start where shear stress is greatest. Its onset depends on the local ratio of equivalent stress to yield strength; the yield index is therefore more informative than shear stress alone.

3. The yield stress ratio is the dominant design parameter. Increasing Ry delays yielding and reduces maximum plastic strain and plastic-zone extent.

4. A thicker hardened layer delays early plastic-zone propagation. Its influence decreases as the cross-section approaches the fully plastic state.

5. Increasing the shear modulus ratio enhances torsional stiffness but may intensify plastic loading. It should be optimized together with the yield stress distribution.

Design of surface-hardened torsional components should consider the local yield index and plastic-zone evolution alongside stress. The formulation provides an efficient framework for graded materials and can be extended to more complex loading and material architectures.

Funding

This research was supported by the Institute of Mechanics and Seismic Stability of Structures named after M.T. Urazbaev, Uzbekistan Academy of Sciences.

References

1. **Padmanabhan, R.; MacDonald, B.J.; Hashmi, M.S.J.** 2004. Elastic-plastic behaviour of an AlSiC MMC rod under combined tension and torsion loading, Journal of Materials Processing Technology 155-156: 1756-1759. https://doi.org/10.1016/j.jmatprotec.2004.04.176.
2. **Mironov, B.G.; Mironov, Yu.B.** 2020. Torsion of Non-Uniform Cylindrical and Prismatic Rods Made of Ideally Plastic Material under Linearized Yield Criterion, Mechanics of Solids 55(6): 813-819. https://doi.org/10.3103/S0025654420060102.
3. **Abirov, R.A.** 2008. On the physical reliability and taking complex loading into account in plasticity, Materials Science 44(4): 512-516. https://doi.org/10.1007/s11003-009-9114-6.
4. **Croné, P.; Gudmundson, P.; Faleskog, J.** 2022. Strain gradient plasticity modelling of cyclic loading in dispersion hardened materials, European Journal of Mechanics - A/Solids 96: 104741. https://doi.org/10.1016/j.euromechsol.2022.104741.
5. **Abirov, R.; Turdibekov, J.** 2026. Axial–Torsional Path Dependence in an Elastoplastic Rod with a Multiply

Connected Cross-Section, Applied Mechanics 7(3): 71. https://doi.org/10.3390/applmech7030071.
6. **Pragya, A.; Ghosh, T.K.** 2023. Soft Functionally Gradient Materials and Structures - Natural and Manmade: A Review, Advanced Materials 35(49): 2300912. https://doi.org/10.1002/adma.202300912.
7. **Qi, C.; Pi, A.G.** 2024. Calculation method for brittle fracture of functional gradient materials, Scientific Reports 14(1): 29262. https://doi.org/10.1038/s41598-024-80884-3.
8. **Singh, P.K.; Kumar, M.; Mishra, S.** 2022. Finite element analysis of functionally graded bar under torsional load, Materials Today: Proceedings 56: 2960-2966. https://doi.org/10.1016/j.matpr.2021.11.012.
9. **Tsiatas, G.C.; Babouskos, N.G.** 2017. Elastic-plastic analysis of functionally graded bars under torsional loading, Composite Structures 176: 254-267. https://doi.org/10.1016/j.compstruct.2017.05.044.
10. **Jiang, Y.; Zhang, R.; Wu, D.; Chen, H.; Gao, W.; Huang, Z.; Zhou, Y.; Zhang, J.; Hu, J.; Luo, G.** 2024. Preparation and Quasi-Isentropic Loading Characteristics of Ti-Pt Periodically Modulated Gradient Material, Chinese Journal of High Pressure Physics 38(6): 064205. https://doi.org/10.11858/gywlxb.20240816.
11. **Akgöz, B.; Civalek, Ö.** 2013. Longitudinal vibration analysis of strain gradient bars made of functionally graded materials (FGM), Composites Part B: Engineering 55: 263-268. https://doi.org/10.1016/j.compositesb.2013.06.035.
12. **Chen, J.F.; Guan, Z.P.; Yang, C.H.; Niu, X.L.; Jiang, Z.T.; Song, Y.Q.** 2018. Comparison of strain ranges and mechanical properties of metal rods under tension and torsion tests, Journal of Jilin University (Engineering and Technology Edition) 48(4): 1153-1160. https://doi.org/10.13229/j.cnki.jdxbgxb20170494.
13. **Abirov, R.A.** 2009. Allowance for complex loading in transversely isotropic solids, Journal of Applied Mechanics and Technical Physics 50(1): 107-111. https://doi.org/10.1007/s10808-009-0015-0.

J.E. Turdibekov, R.A. Abirov, F.F. Adilov

ELASTOPLASTIC TORSION OF A SURFACE-HARDENED FUNCTIONALLY GRADED SQUARE BAR WITH SPATIALLY VARYING MECHANICAL PROPERTIES

S u m m a r y

Surface hardening extends the fatigue life and load-bearing capacity of drive shafts and torque bars. Classical layered models use sharp interfaces, which may introduce stress discontinuities and complicate tracking of plastic-zone evolution. This study develops a continuum model for elastoplastic torsion of a surface-hardened square bar with properties varying continuously from the boundary to the ductile core.

A hyperbolic-tangent transition function describes spatial variations of shear modulus, yield stress, and strain-hardening parameter. The governing differential equation is solved by an iterative Finite Difference Method with harmonic averaging of face stiffness.

The results quantify the effects of material gradients and layer thickness on torque-carrying capacity and plastic-zone evolution. Yielding need not start where shear stress is greatest; its onset is governed by a local yield index. The model supports evaluation and design of surface-treated components under elastoplastic torsion.

Keywords: elastoplastic torsion, surface-hardened bar, functionally graded material, finite difference method, plastic-zone evolution, yield index.

Received July 15, 2026
Accepted October 15, 2026

This article is an Open Access article distributed under the terms and conditions of the Creative Commons Attribution 4.0 (CC BY 4.0) License (http://creativecommons.org/licenses/by/4.0/).